Materials Science & Engineering A 890 (2024) 145991

Contents lists available at ScienceDirect

Materials Science & Engineering A

journal homepage: www.elsevier.com/locate/msea

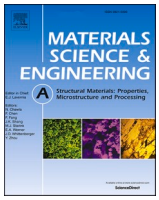

The effect of heat treatment temperature on the mechanical properties of TIMETAL® 575

N.L. Church [a], I.C. James [a], N. Martin [b], N.G. Jones [a,*]

[a] Department of Materials Science and Metallurgy, University of Cambridge, 27 Charles Babbage Road, Cambridge, CB3 0FS, UK
[b] Rolls-Royce plc, PO BOX 31, Derby, DE24 8BJ, UK

A B S T R A C T

TIMETAL® 575 is an α + β alloy reported to possess superior dwell fatigue capabilities over the conventionally used Ti–6Al–4V. The increased performance of this alloy has in part been linked to the presence of fine-scale tertiary α precipitates, which are present in the microstructure following suitable post-forging heat treatments. However, there is currently little understanding as to the extent that these precipitates influence the mechanical properties. When this is coupled with limited information regarding the temperatures over which tertiary α is expected to form, and other microstructural changes which may be occurring concurrent to the evolution of tertiary α in the microstructure, an incomplete picture arises to the true nature of tertiary α on mechanical behaviour. Therefore, this study aims to characterise the mechanical properties of TIMETAL® 575 across a number of different heat treatment temperatures to assess the sensitivity of the mechanical properties on the microstructure.

1. Introduction

α + β titanium alloys are of huge commercial importance to the aerospace sector due to their attractive balance of properties, which include high specific strength, good corrosion resistance and good formability. Typically, these alloys have a bimodal microstructure of α within a β matrix, achieved by a processing route that culminates in sub-transus forging and an α + β heat treatment [1]. Historically, Ti–6Al–4V (Ti64) has been the main alloy of choice for aeroengine components, finding extensive use in fan blade systems, as well as in the discs and blades located within the low-temperature section of the compressor [2]. However, Ti64 is sensitive to cold dwell fatigue, where a significant reduction in fatigue life is observed when a stress hold is introduced, compared to life during conventional fatigue [3]. As such, design of a new alloy for parts of the engine where oscillatory stresses are high, could generate significant advantages [4].

TIMETAL® 575 (Ti575) is a recently developed alloy that aims to provide enhanced strength and fatigue properties when compared to Ti64 [5]. Moreover, the higher specific strength of Ti575 opens up possibilities for the manufacturing of lighter and more compact components [6]. The composition range of Ti575 is protected by a US patent published in 2016 and involves minor compositional adjustments to Ti64 [7]. With a nominal composition of Ti-5.3Al-7.7V-0.5Si-0.25Fe-0.18O, Ti575 contains increased V and reduced Al compared to Ti64, which segregate and strengthen the β and α phases respectively. In addition to this, Ti575 also contains Si to increase the strength and improve the oxidation performance, Fe to further stabilise the β phase, and an increased allowable oxygen content as an interstitial strengthening element. Despite elevated oxygen contents shown to negatively impact dwell fatigue performance [8], it has recently been suggested this phenomenon may only be significant in concentrations above 2500 ppmw [9]. Furthermore, the resulting increase in strength of the alloy may also contribute to a higher fatigue limit [10]. As such, Ti575 has displayed exceptional dwell fatigue properties [8].

Due to the similarity in composition between Ti64 and Ti575, these alloys have demonstrated comparable forging behaviour [6], and it has been suggested that during alloy production, Ti64 may be used as the starting material to significantly reduce cost. However, in addition to the typical bimodal distribution of primary and secondary α commonly observed in Ti64, Ti575 has also been found to possess fine-scale tertiary α precipitates following similar forging treatments. Tertiary α has been reported to form in other systems such metastable β alloys Ti–20Nb–10Zr–5Ta (at.%) [11] and Ti–15Mo–3Al-2.7Nb-0.2Si (at.%) [12], and near-α alloy TA15 (Ti–6Al–2Zr–1Mo–1V (wt%)) where it is thought that their formation is favoured by a high strain energy in the untransformed β lattice [13].

These tertiary precipitates have been proposed as the primary factor responsible for the higher strength of Ti575 whilst maintaining the comparable ductility [14]. Nevertheless, due to the limited number of

* Corresponding author.
E-mail address: ngj22@cam.ac (N.G. Jones).

https://doi.org/10.1016/j.msea.2023.145991
Received 19 October 2023; Received in revised form 21 November 2023; Accepted 6 December 2023
Available online 9 December 2023

studies exploring the impact of microstructure on the mechanical properties of Ti575, the extent to which these precipitates contribute to the overall strength of the alloy remains unclear. This is compounded by the additional effect of the compositional modifications.

This is of additional significance since the microstructural distribution of these precipitates has been observed to vary depending on the solution treatment temperature. In some cases, a preferential formation of tertiary α near to primary α grains has been noted, whilst in others, a more homogeneous distribution throughout the β phase has been observed [15]. Furthermore, following a heat treatment at 700 °C, no tertiary α precipitates were observed at all [5,14]. Consequently, it is necessary to thoroughly characterise the mechanical properties of Ti575 across various microstructural conditions to evaluate the sensitivity of these properties to the microstructure.

Mechanical testing of Ti575 at elevated temperature has suggested a favourable strength compared to Ti64 from ambient conditions up to 700 °C [14]. However, beyond this temperature the strength benefit decreased, with the two alloys showing comparable values. This observation may suggest that tertiary α is an important factor as it is known to be present in the microstructure until at least 500 °C [7]. However, the precise temperature at which tertiary α dissolution occurs, and hence whether this is the controlling factor for the strength up to 700 °C, remains unclear. Furthermore, literature on Ti64 emphasizes the high sensitivity of its mechanical properties to both processing and microstructure, as evidenced by a variation of 200 MPa following a post-forge heat treatment at different temperatures above 700 °C [16,17].

There is evidence of similar microstructure sensitivity in Ti575, as indicated by the variations in reported strength of the alloy in the study covered by the original patent [5]. Variations in strength of close to 100 MPa can be observed between samples heat treated between ~500 and 750 °C. However, as corresponding microstructural information was not given, drawing conclusions about the role of the tertiary α is difficult to distinguish from any changes in the primary and secondary α. Achieving a comprehensive understanding is crucial for the successful design of microstructures optimised to specific applications, and also to understand the alloy's tolerance to microstructural variations.

Hence this study aims to characterise the room temperature and elevated temperature mechanical behaviour of Ti575 across a range of microstructural conditions, achieved by varying the heat treatment temperature. These data will be linked to the corresponding changes in microstructure in each condition to assess the sensitivity of the alloy's mechanical performance to microstructure.

2. Methods

Material for this study was received in the form of a cylindrical forged billet, ~150 mm in diameter and ~30 mm in height, processed to be consistent with [18]. The final forging step had taken place in the α + β region followed by a post-forging heat treatment, to produce a bimodal microstructure of primary and secondary α precipitates, alongside some fine-scale tertiary precipitates. This is henceforth labelled the forged condition. The forged material was then imaged in a number of regions across the billet to ensure consistent microstructural region was used for all subsequent samples. This data is contained within Fig. 1.

Differential scanning calorimetry (DSC) was performed on material in the forged condition by heating and cooling at a rate of 10 °C min^{-1} to a peak temperature of 1100 °C, which is above the reported β transus of Ti575 of 965 ± 5 °C [5]. The sample measured 5 mm in diameter and 1 mm thick, and thermograms were obtained using a Netzsch 404 F1 Pegasus DSC under flowing argon. These data were used to inform the subsequent heat treatment temperatures.

Dogbone type tensile samples, with gauge dimension of 1 × 1.4 mm, and tokens for microstructural characterisation, 10 × 10 × 1 mm, were extracted from the centre of the billet by electro-discharge machining (EDM). These samples were sealed in evacuated quartz ampoules and heat treated for 4 h at six different temperatures of 500, 600, 660, 750, 920 and 1050 °C, followed by a water quench (WQ). After thermal exposure, the tokens were mounted in conductive phenolic resin, ground using successively finer SiC papers, and then polished to a 0.04 μm surface finish using a colloidal silica suspension, buffered to pH 7 with H_2O_2.

Scanning electron microscopy (SEM) was performed using a Zeiss GeminiSEM 300, operated at 15 kV with a 30 μm aperture, with images acquired using back scattered electrons (BSE). Additional micrographs were acquired using BSE imaging in a Hitachi TM4000Plus, operated at 15 kV, with these images used for additional image analysis.

Image analysis was performed using the ImageJ software. Low magnification images (~100 × 100 μm^2 areas) from three separate regions of each token, were used to determine information concerning the primary α phase. Three more regions (~50 × 50 μm^2 areas) were used to analyse the secondary α precipitates. Each precipitate type was isolated and thresholded to determine the area fraction. This methodology is shown in Fig. 2. The tertiary precipitates were not considered due to the difficulty in accurately determining area fraction data. Errors in these values were determined based on the standard deviation in the mean of the three regions considered.

The areas of individual precipitates were statistically binned using the Freedman-Diaconis method [19] and plotted as a histogram for each condition in Wavemetrics IGOR Pro 9. These data were fitted to a log-normal function of the form:

$$y = y_0 + Ae^{-\left(\frac{\ln\left(\frac{x}{x_0}\right)}{w}\right)^2} \quad (1)$$

where y_0 is a constant offset, and A, x_0 and w are fitting functions implemented by IGOR. x_0 and w are related to the geometric mean ($\overline{x}$) of a log-normal distribution and standard error (σ_M) in $\overline{x}$ by:

$$\overline{x} = e^{\ln(x_0)+\frac{w^2}{2}} \quad (2)$$

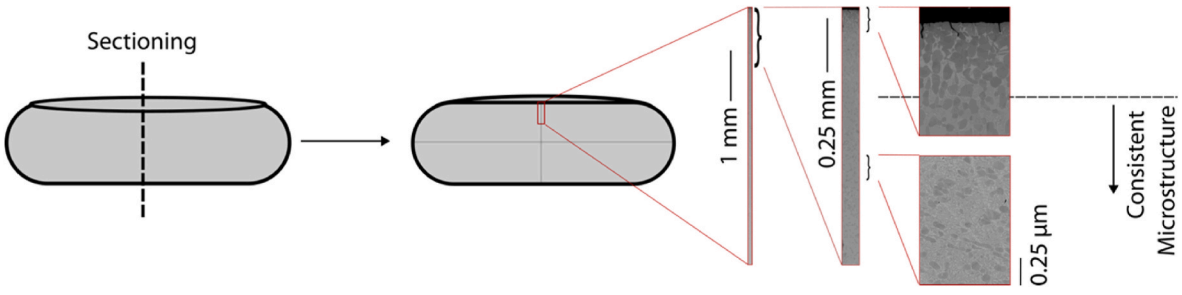

Fig. 1. A schematic diagram showing how the forged billet was sectioned and imaged to ensure all samples were obtained from regions with consistent microstructures.

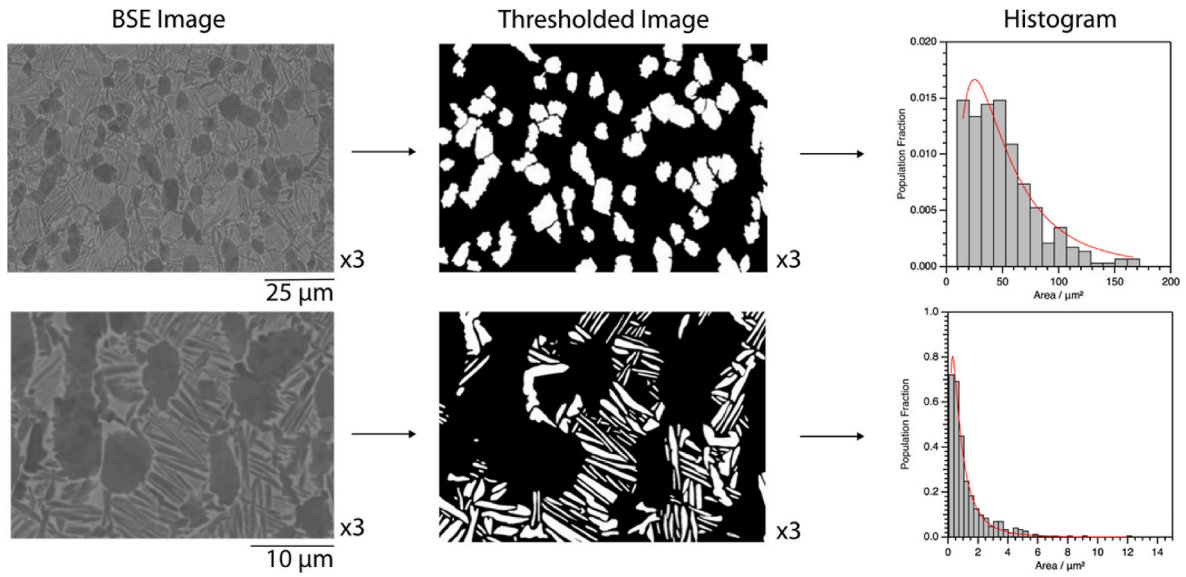

Fig. 2. The methodology used to characterise the size and morphology of the α phase. Top: thresholding of the primary α. Bottom: thresholding of the secondary α.

$$\sigma_M = \frac{e^{\frac{w}{\sqrt{2}}}}{\sqrt{n}} \tag{3}$$

for n precipitates.

To evaluate the morphology of the secondary α, each precipitate was fitted with an ellipse, and the aspect ratio was taken as the ratio between the major and minor axis. These data were plotted as histograms as described above.

X-ray diffraction (XRD) data were acquired using Ni-filtered Cu-Kα radiation using a Bruker D8 ADVANCE diffractometer fitted with a LynxEye EX position sensitive detector. Data were acquired between a 2θ range of 30–80° in increments of 0.02° using a time step of 1 s. Scans were run using a variable slit width, and a constant sample illumination of 5 mm. Each peak, or group of peaks, were fitted to Gaussian functions and lattice parameters were determined from these n peaks through a non-linear least squares minimisation of the sum of weighted squared errors (ξ):

$$\xi = \sum\nolimits_n w_n \left(d_{hkl}^{measured} - d_{hkl}^{calculated}\right)^2 \tag{4}$$

where w_n is the weighting function given by:

$$w_n = \frac{(\sin\theta)^2}{\cos\theta} \tag{5}$$

Mechanical testing was performed on an Instron 3367B test frame with a 30 kN load cell and a 12.5 mm Epsilon contact extensometer. Samples with a gauge cross section of 1.4 mm × 1 mm were pre-loaded to a stress of 25 MPa and tests performed in load control at a rate of 4 MPa s^{-1}, until failure of the sample.

Electro-thermal mechanical testing (ETMT) was used to generate mechanical data at elevated temperature. Samples were resistively heated using a DC supply, with temperature control monitored by an R-type thermocouple spot-welded to the centre of the gauge length. The true strain was determined from the measured resistance before and during deformation using:

$$\varepsilon_t = ln\sqrt{\frac{R}{R_s}} \tag{6}$$

where R_s is the initial starting resistance through the sample, and R is the resistance during deformation. This approach is consistent with that previously used in the literature [20]. This was then converted to engineering strain to be consistent with the stress data and the room temperature mechanical tests.

3. Results

The forged material was assessed to determine the starting microstructural condition for this study, with the corresponding BSE micrographs presented in Fig. 3. The microstructure contained three distributions of the α phase; equiaxed primary α (~10 μm in diameter) plate-like secondary α (~10 μm in length by ~ 1 μm width) and nanoscale acicular tertiary α within the larger regions of the retained β matrix. Such a hierarchical microstructure is highly consistent with previous reports on this alloy.

To identify the solvus temperatures of each population of the α phase, DSC was performed on a sample in the forged condition. The heat flow data recorded during the heating to 1100 °C is presented in Fig. 4. Within this data there was evidence of three distinct endothermic events. Firstly, a low intensity broad event centred around 660 °C, followed by sharper more intense events centred around 880 °C and 940 °C. These three transformation events were hypothesised to correspond to the tertiary, secondary and primary α dissolution respectively and was used as basis for selecting the subsequent heat treatment temperatures. These data were used to select the heat treatment temperatures for the study, which are shown by the blue markers.

To ascertain whether the first thermal event did indeed correspond to the tertiary α dissolving, the microstructure was assessed either side of this broad event, at 500 and 750 °C. Two more conditions of 600 and 660 °C were also considered, which lie within the broad thermal event. These data are shown in Fig. 5.

In all conditions, the samples contained both primary and secondary α in a β matrix. In the material heat treated at 500 °C, nanoscale tertiary α was observed within the β matrix regions. When compared to the initial forged condition, it appears as if the fraction of tertiary α may have increased as a result of the heat treatment but this is difficult to quantify. At 600 °C, tertiary α was still seen in the microstructure, however not in all β channels suggesting the volume fraction had reduced compared to 500 °C. At 660 °C there were only isolated pockets of coarsened tertiary α, consistent with this being the temperature of maximum tertiary α dissolution.

In contrast, there was no evidence of tertiary α in the material that had been heat treated at 750 °C. These observations are consistent with previous studies in the literature, which reported tertiary α in material aged at 500 but none in material aged at 700 °C [14]. Therefore, it is

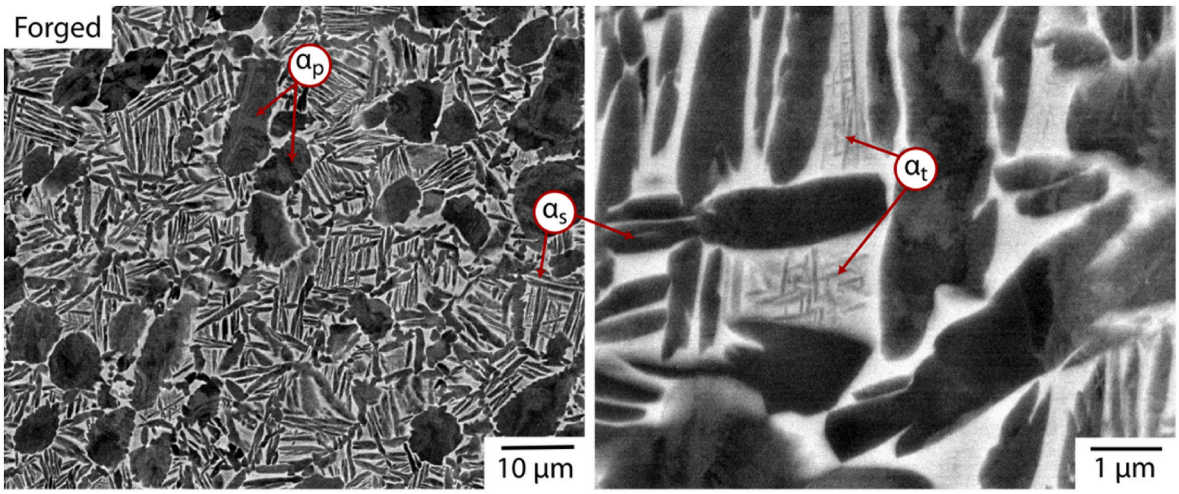

Fig. 3. BSE micrographs of the forged material, showing a microstructure consisting of globular primary α (α_p), lenticular secondary α (α_s) and nanoscale tertiary α (α_t), within a β matrix.

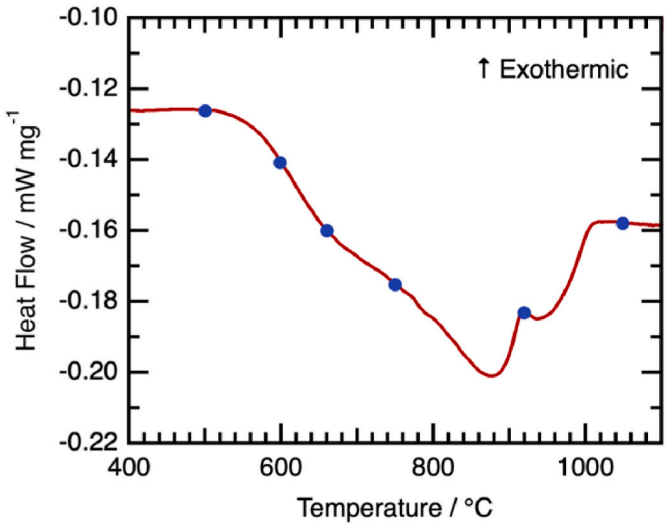

Fig. 4. DSC trace on heating the sample, showing three transformation events. The selected heat treatment temperatures are shown by the blue markers. (For interpretation of the references to colour in this figure legend, the reader is referred to the Web version of this article.)

likely this broad peak in the DSC corresponds to the tertiary α dissolving.

Within the material aged at 750 °C, a number of small dark contrast nanometre-scale features were also observed, typically forming on the secondary α/β boundaries, and highlighted by the red arrows. The darker BSE contrast suggests these features comprise low atomic weight elements. Due to their location, size, and contrast [21], these features may be evidence of silicide formation, however further work is required for unambiguous identification. This temperature is also consistent with the temperature range over which titanium silicide formation is expected [22].

To investigate the higher temperature thermal events, the microstructure of the alloy was also characterised following heat treatments at 920 and 1050 °C. These data are presented in Fig. 6.

Following heat treatment at 920 °C the microstructure still contained the equiaxed primary α but the secondary α appeared to have dissolved into solution. On cooling back to room temperature, a high density of finer, high aspect ratio acicular phase formed within the β matrix. In addition, there was some evidence of a small amount of α forming at the prior β grain boundaries. Following a heat treatment at 1050 °C, none of the original α populations were retained and the microstructure comprised only the fine high aspect ratio phase within the β grains. Consequently, the DSC event at 880 °C likely corresponds to the dissolution of secondary α, with the third thermal event centred on 940 °C, likely corresponding to the dissolution of the primary α. This value corresponds well to the reported β transus temperature in the literature for Ti575 of 965 ± 5 °C [5]. Hence the DSC data can be used to identify all of the phase transformations on heating.

To obtain crystallographic information on the phases in each microstructural condition, XRD data were acquired, and are presented in Fig. 7. All conditions show evidence of BCC and HCP reflections, with no evidence of any other phases. Whilst there is no apparent change in the lattice parameter of the HCP phase, the BCC lattice parameter does appear to vary between samples. Lattice parameters for both phases were determined through a least squares regression, where it was confirmed that those for the HCP phase did not change within error. The lattice parameter for the β phase is given in Fig. 8.

The lattice parameter following a heat treatment at 500 °C decreases compared to the forged condition. This is consistent with the β phase becoming enriched in V and depleted in Al [23], which would suggest an increase in the volume fraction of the α phase. As the heat treatment temperature was increased to 750 °C, the lattice parameter of the β phase also increased, suggesting an enrichment of Al in the β, and therefore a reduced volume fraction of α. This is consistent with the DSC data, suggesting that over this temperature range, the tertiary α dissolves. For heat treatments at higher temperatures, the lattice parameter remains approximately constant suggesting no significant chemical change of the β phase.

Image analysis was performed to study the evolution of the volume fractions of the primary and secondary α as a function of heat treatment temperature and these data are given in Fig. 9. It should be noted that the tertiary α precipitates were too small to accurately quantify through this approach. However, inferences relating to evolution of this population can be made based on the changes in β lattice parameter, compared to any changes in primary and secondary volume fraction. Consequently, the total α fraction presented in Fig. 9 corresponds only to the primary and secondary α precipitates.

Following heat treatment at 500 °C, there was an increase in the total volume fraction of α compared to the forged condition. Based on the image analysis results, this appears to be primarily driven by an increase in the volume fraction of the secondary α. At temperatures between 500 °C and 750 °C, the combination of primary and secondary α volume fraction appeared to be constant within error, highlighting that changes in the β phase lattice parameter are likely driven by a decrease in the

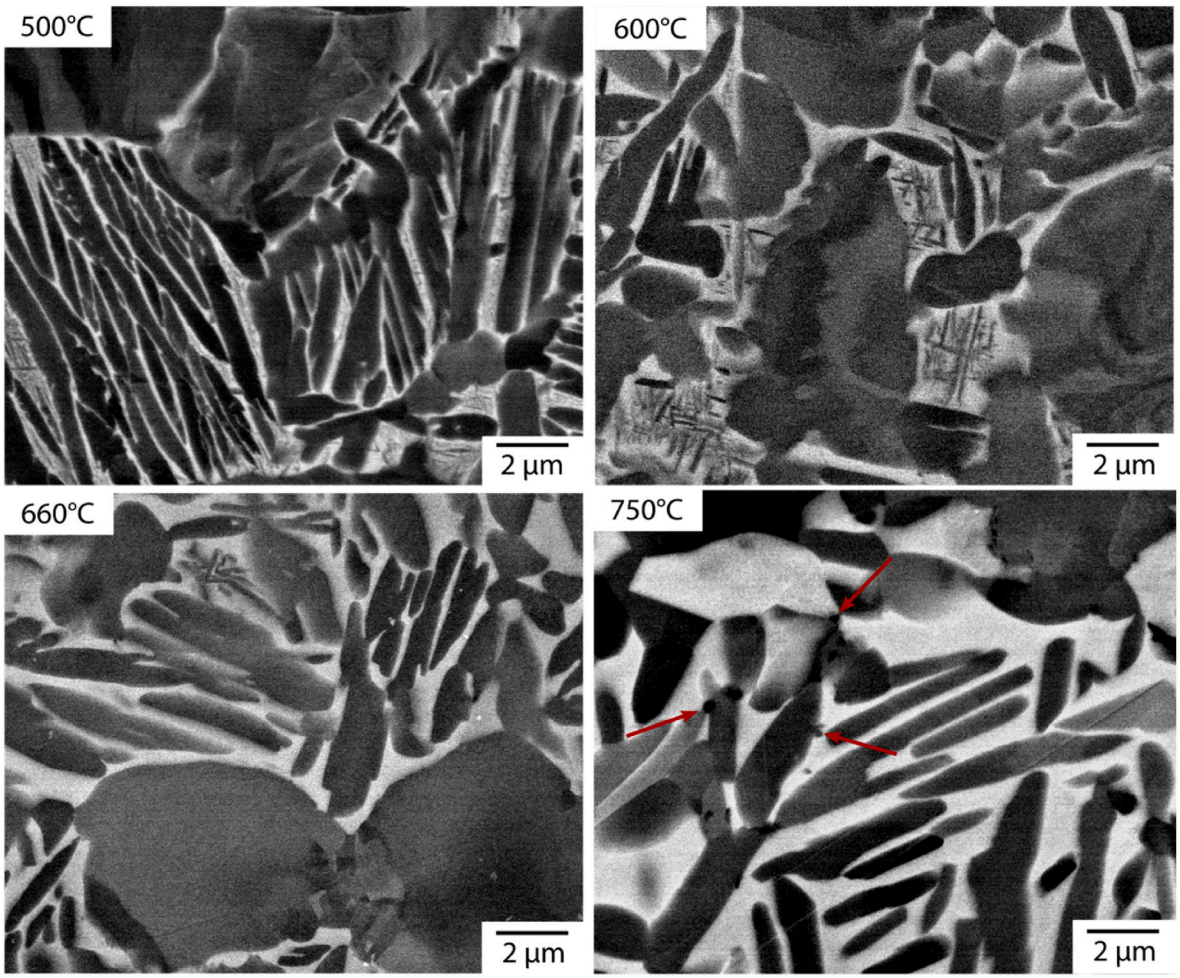

Fig. 5. BSE images of the microstructural condition following heat treatments at 500 600, 660 and 750 °C, which are temperatures spanning the first thermal event in the DSC. The potential silicide formation is highlighted by the red arrows, however this identification requires further work to confirm. (For interpretation of the references to colour in this figure legend, the reader is referred to the Web version of this article.)

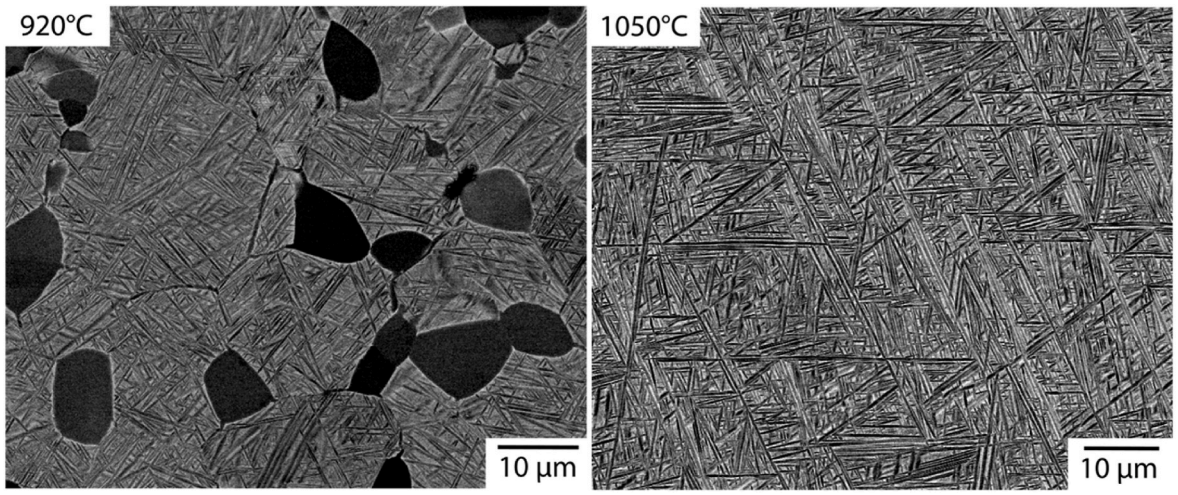

Fig. 6. BSE images of the microstructures following heat treatments above the second and third thermal events in the DSC.

tertiary volume fraction. Following heat treatments at 920 °C and 1050 °C, the secondary then primary α volume fractions decrease to 0 as expected.

The size of the primary and secondary α precipitates are given in Fig. 10. For heat treatments up to 750 °C, the size of both the primary and secondary α increases. As the volume fraction is unchanged, this is consistent with a coarsening of the precipitates. At 920 °C there is a drop in the primary α size, which is consistent with β approach curve in literature for Ti575 [14] that highlighted a decrease in the amount of primary α in microstructure at temperatures above 910 °C.

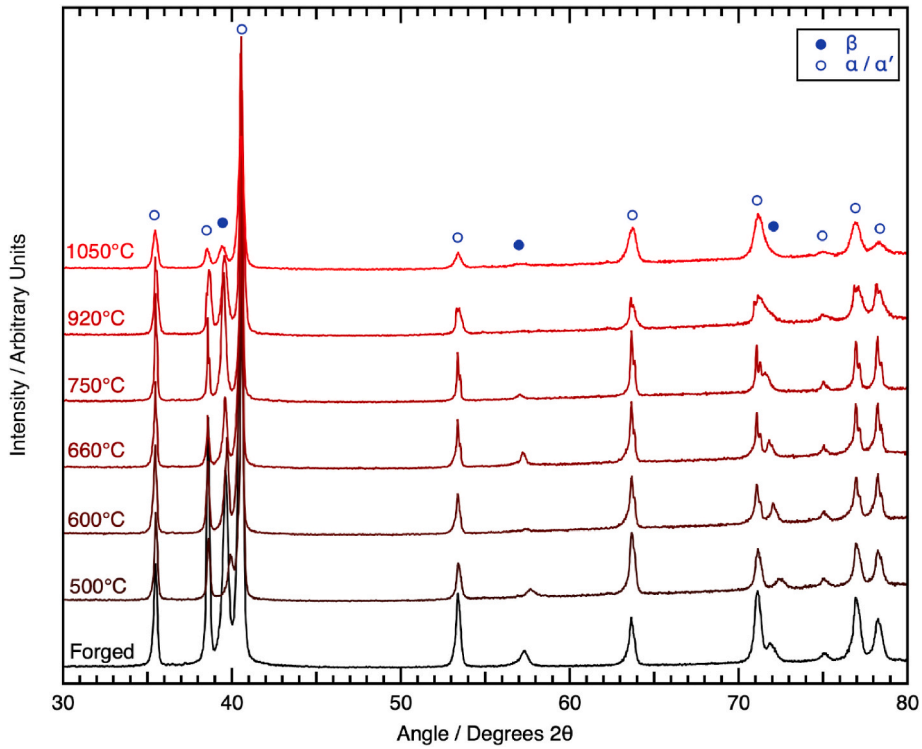

Fig. 7. XRD data showing the phases present at room temperature following heat treatments at various temperatures.

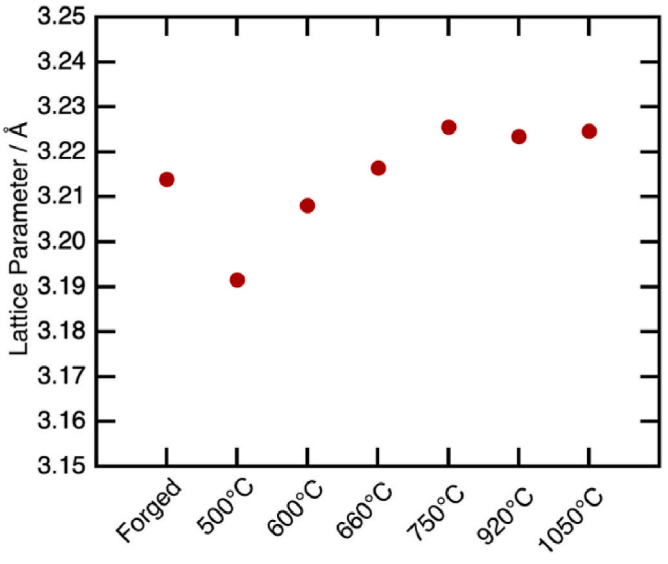

Fig. 8. Variation in the room temperature lattice parameter of the β phase following heat treatments at various temperatures.

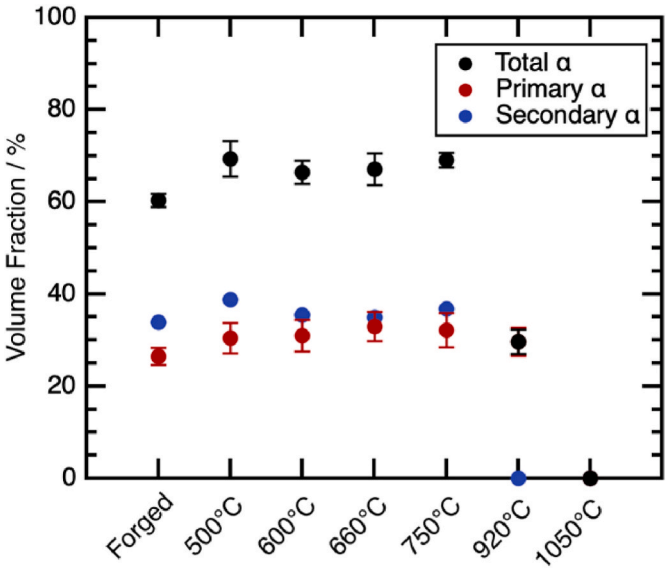

Fig. 9. Area fraction of the α phase following heat treatments at different temperatures. The total α fraction is a combination of primary and secondary α, with the fraction of tertiary α not considered due to the difficulty in accurately determining the fraction of such small precipitates.

As the change in size of the secondary α suggests coarsening, the precipitates were further analysed to determine whether their aspect ratio was also evolving. This data is given in Fig. 11 and showed a decrease in the aspect ratio of the secondary α following heat treatments at higher temperatures. Again, this is consistent with a coarsening of the secondary α precipitates.

The mechanical properties of the alloy in each microstructural condition were assessed through uniaxial tensile tests, with these data presented in Fig. 12. Following a heat treatment at 500 °C, there was a modest increase in strength, with no loss in ductility. However, following heat treatment at higher temperatures, up to 750 °C, the strength of the material decreased. This was coupled with a decrease in the ductility of the samples, which was particularly evident following a heat treatment at 750 °C. For heat treatment temperatures above 750 °C, the room temperature strength increased, with a decrease in ductility compared to the forged condition. However, this change in behaviour may be related to the fine acicular phase observed in the corresponding microstructures, that was believed to form on cooling.

To assess the elevated temperature deformation behaviour, mechanical testing was also performed in an ETMT. The resulting stress-strain data are shown in Fig. 13. There was a clear decrease in

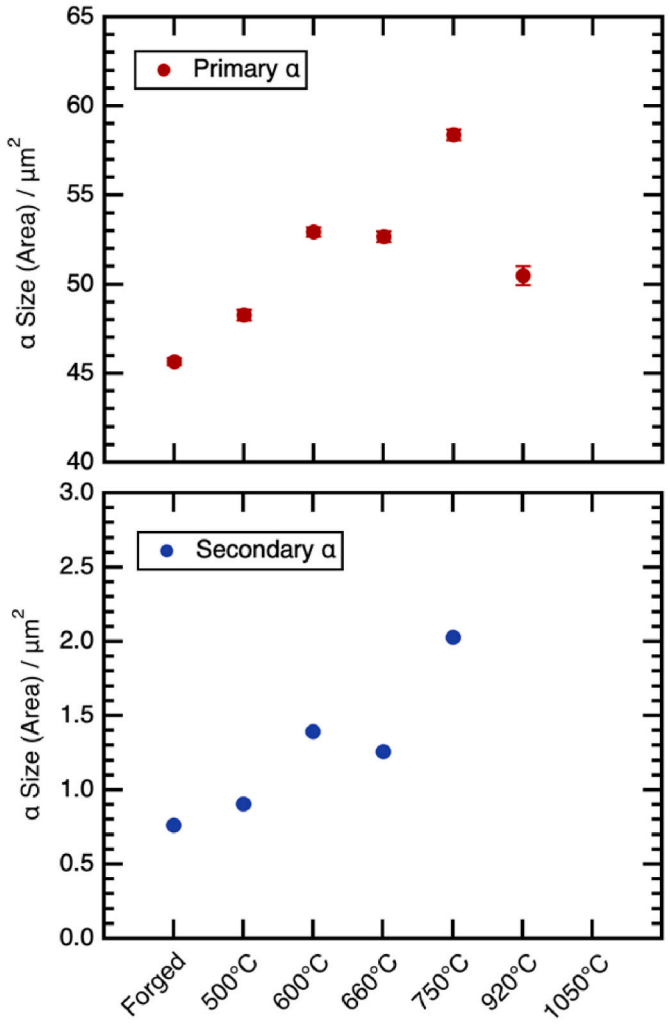

Fig. 10. Size of the primary and secondary α precipitates for different heat treatment conditions.

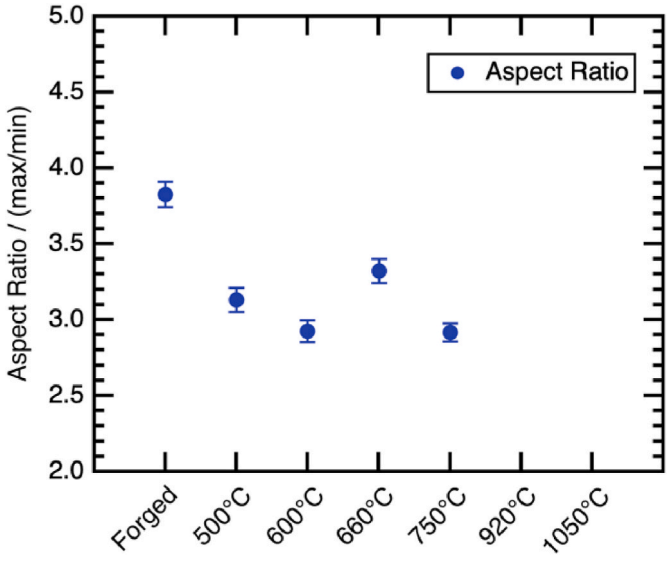

Fig. 11. The aspect ratio of the secondary α for different heat treatment conditions.

strength as the testing temperature was increased, which is expected given that dislocation mobility is a temperature activated process. However, inferences can be made as to the effect of tertiary α when considering the extent of this decrease in strength as a function of temperature. For example, the room temperature strength following the heat treatment at 600 °C was comparable to the initial forged condition, whilst in the elevated temperature tests, it was significantly decreased to ~300 MPa. Both of these conditions contained tertiary α. In the ETMT test performed at 750 °C, when the tertiary α was removed, the decrease in strength followed a similar trend to the previous temperatures, suggesting no dramatic effect from the removal of the tertiary α. At even higher temperatures, the strength is very low, with very large elongations observed within the ETMT. This is consistent with superplastic deformation behaviour. The values observed at these higher temperatures are lower than literature [14], however ease of superplastic deformation is sensitive to grain size [24] and so these datasets are not inconsistent.

4. Discussion

A number of microstructural conditions were obtained by varying the heat treatment temperature, and these were used to assess the effect of different microstructural features on the mechanical properties of Ti575. The temperatures were selected to include a heat treatment above the β transus temperature, between the primary and secondary α thermal events, between the secondary and tertiary α thermal events and for three lower temperatures across and below the tertiary α event, which will therefore result in different tertiary α volume fractions. The phases present, volume fractions and room temperature mechanical properties are summarised in Table 1.

For heat treatment temperatures between 500 °C and 750 °C, both the strength and ductility decreased as the temperature was raised. For 920 °C and 1050 °C, the strength increased, whilst the ductility was reduced compared to the forged condition. The increase in strength for 920 °C and 1050 °C was not evident in the tests at elevated temperature, and as such it is likely the higher strength here is related to the formation of the high aspect ratio phase on quenching.

This phase was shown to have an HCP crystallography, and as such could be either α or the α′ martensite, which are challenging to distinguish via lab-based XRD techniques. Due to an ~1 μm interaction volume, compositional separation between the β and the reformed phase was not possible, however the likely identity of this phase can be inferred based on the literature of Ti64. The formation of α′ martensite is highly affected by cooling rate, with similar heat treatments and cooling rates in the literature shown to form α′ when WQ from above the β transus, and α′ alongside a small amount of α when WQ from just below the transus temperature [25]. This is consistent with only the lenticular phase present in the microstructure when cooled from 1050 °C, however a lenticular phase and some grain boundary α formation when cooled from 920 °C. α′ is known to increase the hardness and reduce the ductility of α + β alloys and so its presence within the microstructure would rationalise the observed differences in mechanical behaviour [26]. At elevated temperature, the α′ will not be present, and hence a much lower strength is seen in the material.

In bimodal microstructures of Ti64, attention has frequently been paid to the deformation behaviour of the primary α phase, as the combination of finer secondary α in the β matrix is believed to make these regions less deformable [27 – 30]. As such, it is important to consider the potential effect of any changes in the primary α size and volume fraction.

In the present study there was evidence to suggest a small increase in the primary α volume fraction between the forged and 500 °C condition. This coincides with an increase in strength of the material. Comparing the microstructures in Fig. 3 and Fig. 5, there appears to be an increase in the volume fraction of the tertiary α, with precipitates seen in the majority of the retained β regions, compared to primarily the larger regions before the heat treatment. An increase in the tertiary volume

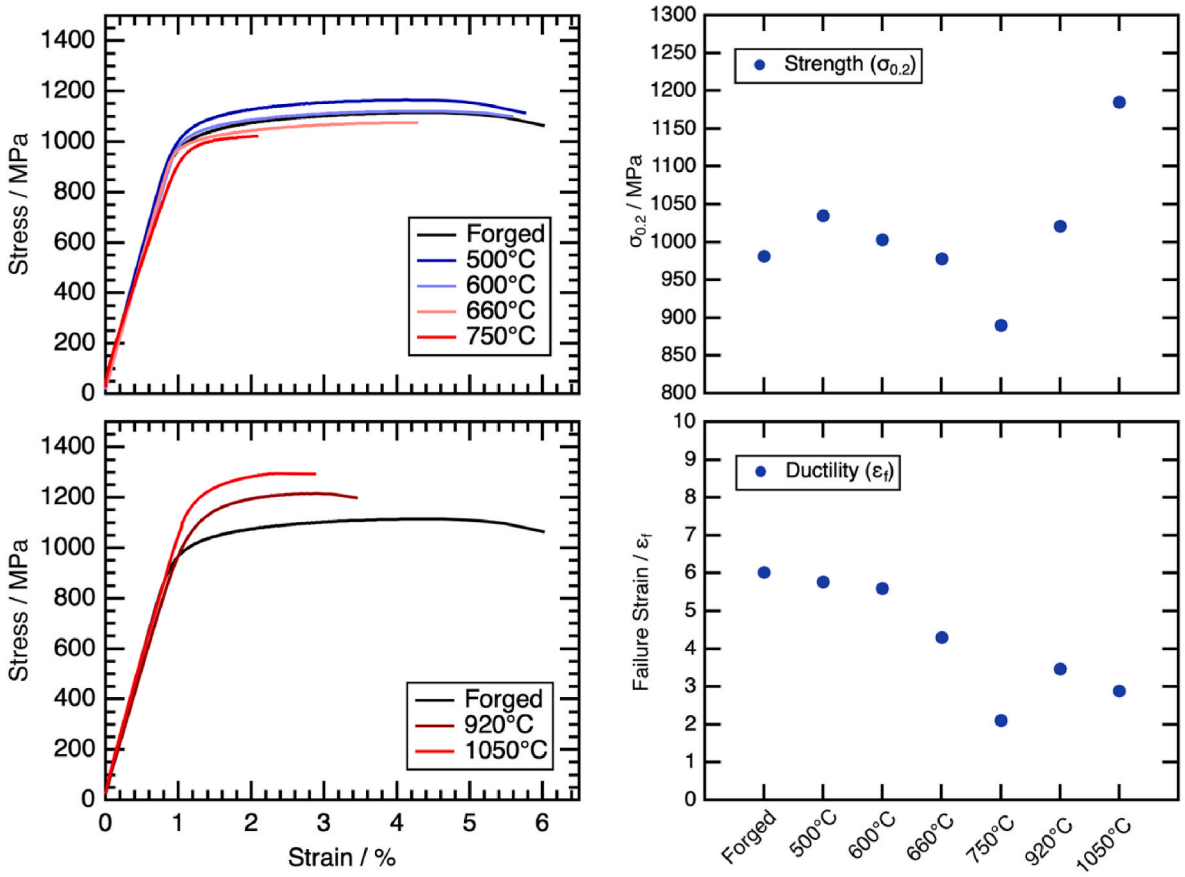

Fig. 12. The room temperature mechanical behaviour of the samples following heat treatments at different temperatures. Left: the tensile curves to failure for each sample. Right: the strength and ductility of the samples.

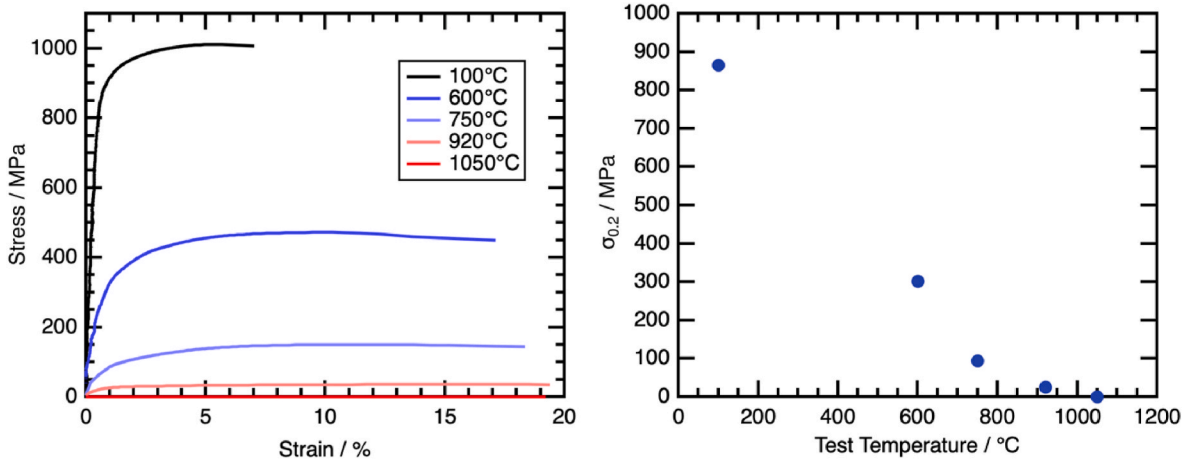

Fig. 13. Mechanical testing at elevated temperature alongside a plot of the yield strength as a function of temperature.

fraction would be consistent with the observed change in mechanical response, and consistent with literature reports that the tertiary α is important for strength. However, the change in strength of only 54 MPa, despite an increase in both primary and tertiary α volume fraction suggests the contribution of the tertiary α is small.

There may have been a small decrease in primary α volume fraction for the 920 °C condition evidenced by the decrease in primary α size, although these variations remained within the measurement error. In all other conditions the volume fraction remained comparable to the 500 °C condition. Considering the general increase in primary α size for these temperatures up to 750 °C, the primary α is likely coarsening slightly during the heat treatment. This coarsening will likely cause a small decrease in strength of the alloy between 500 °C and 750 °C [1], which matches well with the observed trend.

Between 500 °C and 750 °C, the secondary α precipitates also remain at a constant volume fraction. However, the concurrent increase in size and decrease in aspect ratio similarly suggests coarsening. This effect is likely to be more pronounced as the initially high aspect ratio of the secondary α suggests an increased driving force for coarsening. In related literature it has been shown that as the aspect ratio decreases, the

Table 1
Summary of the microstructural features, alongside the room temperature mechanical properties.

	Forged	500 °C	600 °C	660 °C	750 °C	920 °C	1050 °C
Primary α Frac./%	26.5 ± 1.9	30.4 ± 3.3	30.9 ± 3.4	33.0 ± 3.2	32.1 ± 3.7	29.6 ± 3.1	–
Secondary α Frac./%	33.8 ± 0.6	38.8 ± 0.7	35.5 ± 0.7	34.9 ± 0.9	36.8 ± 0.9	–	–
Tertiary α Rel. Frac.	Med	High	Med	Low	–	–	–
Primary α Size/μm^2	45.6 ± 0.2	48.2 ± 0.3	52.9 ± 0.3	52.6 ± 0.3	58.4 ± 0.3	50.5 ± 0.5	
Secondary α Size/μm^2	0.762 ± 0.003	0.904 ± 0.005	1.392 ± 0.008	1.259 ± 0.007	2.029 ± 0.006	–	–
Secondary α Aspect Ratio	3.83 ± 0.08	3.13 ± 0.08	2.92 ± 0.07	3.32 ± 0.08	2.91 ± 0.06	–	–
Strength ($\sigma_{0.2}$)/MPa	981	1035	1003	978	890	1021	1185
Failure Strain/%	6.02	5.77	5.60	4.29	2.10	3.46	2.89

strength decreases [31,32] due to an increase in the effective slip length [1]. Again, this trend matches well to the observed decrease in strength.

The tertiary precipitates decrease in volume fraction between 500 °C and 750 °C, and this correlates with a decrease in the strength and ductility of the sample. The literature suggests that tertiary α may be important for these properties, which would be consistent with this trend. However, the changes in strength across this temperature range remain small, varying but ~30 MPa between each condition. This will result from a combination of the coarsening of primary and secondary alpha, and removal of the tertiary precipitates. As such the true contribution to strength from the tertiary precipitates is only small.

At elevated temperatures, the strength of Ti575 is shown to decrease as the test temperature increased, which is expected given that slip is a thermally activated process. The measured yield stresses are consistent with those reported in the originally patent [7], and captures the same trends. The yield stress of Ti64 has been shown to decrease by ~400 MPa between room temperature and 500 °C, with an associated increase in ductility [33]. This is a comparable decrease to the current work, despite Ti64 containing no tertiary α. As such, the tests at elevated temperature suggest comparable behaviour between both alloys, despite Ti575 containing tertiary precipitates at lower temperatures.

At the higher temperatures of 920 and 1050 °C, the yield stress of the alloy is particularly low, and this is not captured by literature trends for Ti575. However, these stresses are not inconsistent with superplastic deformation [1], which is known to be influenced by microstructural features such as grain size [34].

The magnitude of increase in strength between the forged condition and the 500 °C condition is low, and the decrease in strength thereafter includes contributions from the coarsening of the primary and secondary α, with similar trends seen in Ti64. As such, whilst tertiary α is undoubtedly contributing to the strength of the alloy, it's affect does not appear to be particularly dramatic.

5. Conclusion

By analysing the calorimetry data for material in the forged condition, the key transformation temperatures for Ti575 were able to be determined. These data show that dissolution of the tertiary α occurred between ~550 and 750°, which was confirmed through microstructural analysis.

A number of microstructural conditions of Ti575 were tested at both room temperature and elevated temperature to assess the sensitivity of the microstructure on the alloy's mechanical properties, and to determine the extent of the role that tertiary α contributes to strength. An increased tertiary α volume fraction was seen to have a positive effect on the strength, and a loss of tertiary α coincided with a decrease in strength. However, the decrease in strength as the tertiary α dissolved was small, varying by ~30 MPa between conditions. Other factors such as coarsening of the primary and secondary α precipitates will also have contributed to this decrease. Furthermore, the observed trends were shown to be consistent with those of Ti64, despite Ti64 not containing tertiary α.

As such, whilst the literature has demonstrated that Ti575 can possess favourable dwell fatigue properties, given suitable processing schedules, the tensile strength and ductility of the alloy has been shown to offer limited improvements over Ti64. The sensitivity of mechanical properties on the microstructure appears comparable to Ti64 however must be thoroughly characterised before widescale industrial application.

CRediT authorship contribution statement

N.L. Church: Formal analysis, Investigation, Methodology, Validation, Visualization, Writing – original draft. **I.C. James:** Formal analysis, Investigation. **N. Martin:** Conceptualization, Resources, Writing – review & editing. **N.G. Jones:** Conceptualization, Formal analysis, Funding acquisition, Investigation, Methodology, Project administration, Resources, Supervision, Validation, Writing – original draft.

Declaration of competing interest

The authors declare that they have no known competing financial interests or personal relationships that could have appeared to influence the work reported in this paper.

Data availability

The underlying research data required to reproduce these findings are available from the University of Cambridge repository (10.17863/CAM.100157).

Acknowledgements

The authors are grateful to Rolls-Royce plc. for supplying the material for this work. The authors would also like to thank Dr H.T. Pang for his assistance with data collection, and Dr G.J. Wise for his assistance with data processing.

References

[1] G. Lutjering, J. Williams, Titanium, Spiringer, 2007.
[2] I. Inagaki, Y. Shirai, T. Takechi, N. Ariyasu, Application and Features of Titanium for the Aerospace Industry, 2014. https://www.nipponsteel.com/en/tech/report/nssmc/pdf/106-05.pdf. (Accessed 17 November 2023).
[3] Z. Wu, H. Kou, N. Chen, Z. Xi, J. Fan, B. Tang, J. Li, Recent developments in cold dwell fatigue of titanium alloys for aero-engine applications: a review, J. Mater. Res. Technol. 20 (2022) 469–484, https://doi.org/10.1016/j.jmrt.2022.07.094.
[4] L.W. Meyer, L. Krüger, K. Sommer, T. Halle, M. Hockauf, Dynamic strength and failure behavior of titanium alloy Ti-6Al-4V for a variation of heat treatments, Mech. Time-Dependent Mater. 12 (2008) 237–247, https://doi.org/10.1007/s11043-008-9060-y.
[5] M. Thomas, J. Hewitt, M. Bache, R. Thomas, P. Garratt, Y. Kosaka, Determination and analysis of the cyclic and dwell fatigue performance of Timetal® 575, in: Proceedings of the 13th World Conference on Titanium, 2016, pp. 979–984, https://doi.org/10.1002/9781119296126.ch167.
[6] S. Andrieu, I. von Thüngen, A. Lenain, Y. Millet, Ti575: a new timet alloy for structural parts in aeronautics, in: Proceedings of the 13th World Conference on Titanium, 2016, pp. 1543–1546, https://doi.org/10.1002/9781119296126.ch258.
[7] S. Thomas, Y. Coldfield, H. Kosaka, High Strength Alpha Beta Titanium Alloy, 2013.
[8] Y. Xiong, P.S. Karamched, C.T. Nguyen, D.M. Collins, N. Grilli, C.M. Magazzeni, E. Tarleton, A.J. Wilkinson, An in-situ synchrotron diffraction study of stress relaxation in titanium: effect of temperature and oxygen on cold dwell fatigue, Acta Mater 213 (2021) 116937, https://doi.org/10.1016/j.actamat.2021.116937.

[9] F.F. Worsnop, R.E. Lim, J.V. Bernier, D.C. Pagan, Y. Xu, T.P. McAuliffe, D. Rugg, D. Dye, The influence of alloying on slip intermittency and the implications for dwell fatigue in titanium, Nat. Commun. 13 (2022) 5949, https://doi.org/10.1038/s41467-022-33437-z.
[10] H. Arabi, Effect of tensile strength on fatigue behaviour and notch sensitivity of Ti-6Al-4V, Iranian Journal of Materials Science 2 (2005) 1–4.
[11] R. Banerjee, S. Nag, H.L. Fraser, A Novel Combinatorial Approach to the Development of Beta Titanium Alloys for Orthopaedic Implants, Materials Science and Engineering C, 2005, pp. 282–289, https://doi.org/10.1016/j.msec.2004.12.010.
[12] H. Jiang, Z. Du, D. Wang, T. Gong, X. Cui, F. Liu, J. Cheng, W. Chen, Preparation of multiscale α phase by heat treatments and its effect on tensile properties in metastable β titanium alloy sheet, Metals 11 (2021) 1708, https://doi.org/10.3390/met11111708.
[13] Z. Sun, X. Li, H. Wu, H. Yang, Morphology evolution and growth mechanism of the secondary Widmanstatten α phase in the TA15 Ti-alloy, Mater. Char. 118 (2016) 167–174, https://doi.org/10.1016/j.matchar.2016.05.020.
[14] M. Thomas, J. Hewitt, M. Bache, R. Thomas, P. Garratt, Y. Kosaka, Timetal® 575: a novel high strength forgeable α/β titanium alloy, in: Proceedings of the 13th World Conference on Titanium, 2016, pp. 1537–1541, https://doi.org/10.1002/9781119296126.ch257.
[15] E. Frutos-Myro, I. MacLaren, P. Li, I. Berment-Parr, M. Thomas, Nano-scale characterisation of tri-modal microstructures in TIMETAL ® 575, MATEC Web of Conferences 321 (2020), 12025, https://doi.org/10.1051/matecconf/202032112025.
[16] R.R. Boyer, Titanium and its alloys: metallurgy, heat treatment and alloy characteristics, in: Encyclopedia of Aerospace Engineering, John Wiley & Sons, Ltd, 2010, https://doi.org/10.1002/9780470686652.eae198.
[17] W.-S. Lee, C.-F. Lin, Plastic Deformation and Fracture Behaviour of Ti-6Al-4V Alloy Loaded with High Strain Rate under Various Temperatures, Mater. Sci. Eng. A 1-2 (1998) 48 -59, doi: 10.1016/S0921-5093(97)00471-1.
[18] M. Bodie, M. Thomas, A. Ayub, Effect of microstructure and cooling rate on the fatigue performance of TIMETAL ® 575, MATEC Web of Conferences 321 (2020), 12019, https://doi.org/10.1051/matecconf/202032112019.
[19] D. Freedman, P. Diaconis, On the Histogram as a Density Estimator: L 2 Theory, Z. Wahrscheinlichkeitstheorie verw, Gebiete 57 (1981) 453–476, https://doi.org/10.1007/BF01025868.
[20] B. Roebuck, D.C. Cox, R.C. Reed, AN INNOVATIVE DEVICE FOR THE MECHANICAL TESTING OF MINIATURE SPECIMENS OF SUPERALLOYS, Superalloys2004, TMS, 2004.
[21] C. Fleißner-Rieger, H. Schönmaier, M. Musi, M. Stadler, H. Gschiel, C. Turk, T. Pfeifer, H. Clemens, Formation and evolution of precipitates in an additively manufactured near-α titanium base alloy, Materialia (Oxf). 21 (2022), https://doi.org/10.1016/j.mtla.2022.101366.
[22] C. Nobili, F. Nava, G. Ottaviani, M. Costato, G. De Santi, G. Queirolo, Titanium Silicide Formation in Presence of Oxygen, Active and Passive Electronic Components 15 (1992), 094394, https://doi.org/10.1155/1992/94394.
[23] J.W. Elmer, T.A. Palmer, S.S. Babu, E.D. Specht, In situ observations of lattice expansion and transformation rates of α and β phases in Ti-6Al-4V, Mater. Sci. Eng. 391 (2005) 104–113, https://doi.org/10.1016/j.msea.2004.08.084.
[24] E.W. Collings, The Physical Metallurgy of Titanium Alloys, American Society for Metals, 1984.
[25] A. Shaikh, S. Kumar, A. Dawari, S. Kirwai, A. Patil, R. Singh, Effect of temperature and cooling rates on the α+β morphology of Ti-6Al-4V alloy, in: Procedia Structural Integrity, Elsevier B.V., 2019, pp. 782–789, https://doi.org/10.1016/j.prostr.2019.07.056.
[26] P.O. Omoniyi, E.T. Akinlabi, R.M. Mahamood, Heat treatments of Ti6Al4V alloys for industrial applications: an overview, in: IOP Conf Ser Mater Sci Eng., vol. 1107, 2021, 012094, https://doi.org/10.1088/1757-899x/1107/1/012094.
[27] H. Li, D.E. Mason, Y. Yang, T.R. Bieler, M.A. Crimp, C.J. Boehlert, Comparison of the deformation behaviour of commercially pure titanium and Ti-5Al-2.5Sn(wt.%) at 296 and 728 K, Phil. Mag. 93 (2013) 2875–2895, https://doi.org/10.1080/14786435.2013.791752.
[28] H. Li, C.J. Boehlert, T.R. Bieler, M.A. Crimp, Analysis of the deformation behavior in tension and tension-creep of Ti-3Al-2.5V (wt pct) at 296 K and 728 K (23 °C and 455 °C) using in situ SEM experiments, Metall Mater Trans A Phys Metall Mater Sci 45 (2014) 6053–6066, https://doi.org/10.1007/s11661-014-2576-7.
[29] F. Bridier, P. Villechaise, J. Mendez, Analysis of the different slip systems activated by tension in a α/β titanium alloy in relation with local crystallographic orientation, Acta Mater. 53 (2005) 555–567, https://doi.org/10.1016/j.actamat.2004.09.040.
[30] H. Li, D.E. Mason, T.R. Bieler, C.J. Boehlert, M.A. Crimp, Methodology for estimating the critical resolved shear stress ratios of α-phase Ti using EBSD-based trace analysis, Acta Mater. 61 (2013) 7555–7567, https://doi.org/10.1016/j.actamat.2013.08.042.
[31] Y. Liu, F. Chen, G. Xu, Y. Cui, H. Chang, Correlation between microstructure and mechanical properties of heat-treated Ti–6Al–4V with Fe alloying, Metals 10 (2020) 1–15, https://doi.org/10.3390/met10070854.
[32] Y. Ren, S.M. Zhou, Z.Y. Xue, W.B. Luo, Y.J. Ren, Y.J. Zhang, Effect of α-platelet thickness on the mechanical properties of Ti-6Al-4V alloy with lamellar microstructure, in: IOP Conf Ser Mater Sci Eng, Institute of Physics Publishing, 2017, https://doi.org/10.1088/1757-899X/281/1/012024.
[33] S. Kumar, K. Chattopadhyay, V. Singh, Tensile behavior of Ti-6Al-4V alloy at elevated temperatures, in: Proceeding of the International Conference on Multifunctional Materials, Structures and Applications, 2014. https://www.researchgate.net/publication/308787239.
[34] D. Yin, G. Qin, K. Cao, Research status of influencing factors on superplastic properties of titanium alloy, in: IOP Conf Ser Earth Environ Sci, IOP Publishing Ltd, 2020, https://doi.org/10.1088/1755-1315/598/1/012065.